Date of publication mmmm dd, yyyy, date of current version mmmm dd, yyyy.

Digital Object Identifier aa.bbbb/ACCESS.2022.DOI

Quantum Processing in Fusion of SAR and Optical Images for Deep Learning: A Data-Centric Approach

SATHWIK REDDY MAJJI[1], (Student Member, IEEE), AVINASH CHALUMURI[1], (Graduate Student Member, IEEE), RAGHAVENDRA KUNE[2], and B. S. MANOJ[1], (Senior Member, IEEE),

[1]Indian Institute of Space Science and Technology, Kerala, India
[2]Advanced Data Processing Research Institute, Telangana, India

Corresponding author: B. S. Manoj (e-mail: bsmanoj@ieee.org).

This work is funded in parts by IIT Palakkad Technology IHub Foundation Doctoral Fellowship IPTIF/HRD/DF/032.

ABSTRACT Deep learning techniques are very prominent in processing remotely sensed synthetic aperture radar (SAR) images for real-time, high-impact applications, such as image classification, object detection, and semantic segmentation. The accuracy of deep learning models, such as convolutional neural networks (CNNs), depends on the quality of the input data. Compared to the model-centric approach, where the model parameters are optimized during training, the data-centric approach can enhance the performance accuracy as data quality is improved before training the models. Improving the data quality of SAR images is challenging as SAR image properties are different from optical (OPT) images. Image fusion techniques proved to enhance the quality of SAR images when combined with OPT images. Many fusion techniques exist for combining SAR and OPT images in the classical domain. This paper proposes a novel approach to using quantum computing for the image fusion of SAR and OPT images. Eight different quantum processing techniques are used for the fusion of the images. We designed and created a dataset for land-use classification by collecting data using the Google Earth Engine. The quality metric measurements show that the quality of SAR images has improved by using the proposed quantum processing techniques. In addition, performance evaluation of the deep learning CNNs on the dataset was carried out for all quantum processing techniques. Our approach improved the classification accuracy from 82.64%, with only SAR images for training, to 95.36% using the proposed image fusion techniques.

INDEX TERMS quantum processing, image fusion, deep learning, image classification, synthetic aperture radar (SAR) imagery, optical imagery.

I. INTRODUCTION

THE deep learning (DL) technique has a tremendous ability to solve supervised machine learning problems [1]. The two main components of supervised machine learning algorithms are the data and the model. For supervised learning, input data and output labels are used to train the model and build classification models. The model parameters are optimized using a loss function, and hyperparameters are tuned to build a model that performs classification with high accuracy. As data and model are the essential components in the algorithm, two main approaches are used to tune the model. The first is the model-centric approach, in which input data is kept unchanged, and the architecture of the model is tuned by changing the hyper-parameters to achieve the required performance. The second is a data-centric approach, where a dataset is systematically changed or enhanced to improve the learning performance of the model. In any case, the accuracy and performance mainly depend on the quality of input data. As deep learning models are trained on large amounts of data, data-centric approaches can be effective as the input data is improved for training the models [2]. The data-centric approach is also used to improve label consistency, fine sampling of data, and batch selection [3].

Currently, most DL applications are model-centric, and most research focuses on designing and improving the models with the same data used for training the models. Accord-

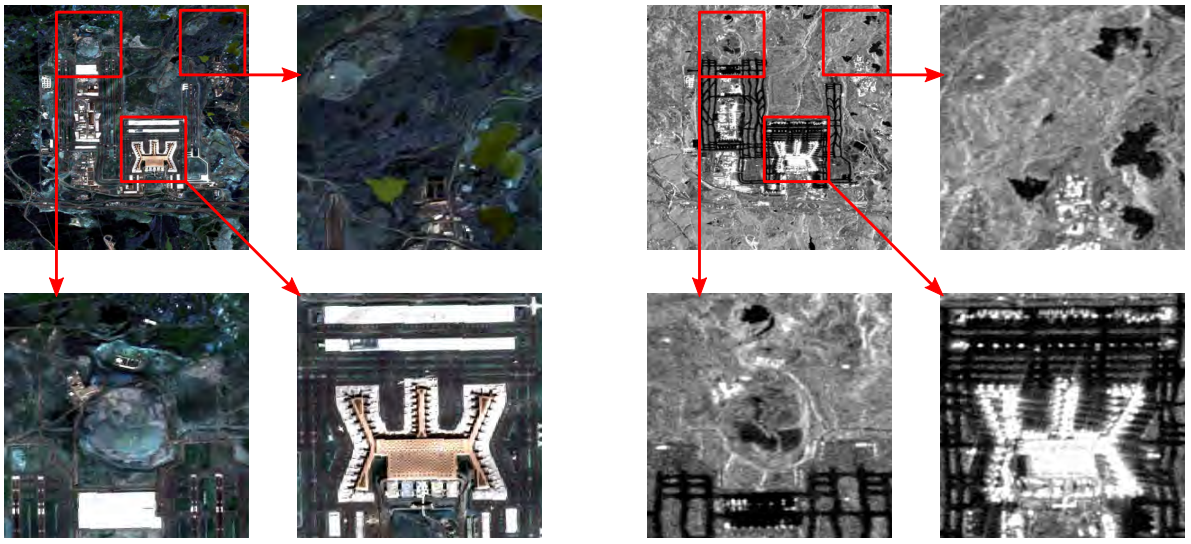

(a) Optical image with three subscenes

(b) SAR image with three subscenes

FIGURE 1. Comparison between optical and SAR images of same area from Google Earth Engine (GEE).

ing to Andrew Ng, more than 90% of research papers in this domain are model-centric [4]. The main reason for focusing on the model-centric approach is that creating large datasets with good standards is difficult. As a result, the model-centric approach is believed to be more effective as data collection is considered a one-time event. Also, improving data quality is an important research that needs further work.

However, tremendous improvements in the accuracy are observed using the data-centric approaches such as improving the data quality, consistency of the labels, finely sampling the training data, and choosing the batches wisely [3]. Especially in remote sensing applications, increasing data quality for training deep learning models can build accurate models. Remote sensing involves gathering information about objects, and features on the land surface, oceans, and the atmosphere with the help of sensors located far beyond the vicinity of such source. Many remote sensing satellites deployed by multiple agencies orbit the Earth and make a large information bank available. Therefore, applying data-centric approaches can be constructive in dealing with remote sensing data. However, before choosing a data-centric approach, data properties are to be considered. Remotely sensed information in synthetic aperture radar (SAR) images is different from optical (OPT) images. For example, as shown in the sub-scenes of Fig. 1, roadways in SAR imagery can be observed clearly in comparison with OPT images. However, objects such as airport buildings can be visually identified in OPT images than in SAR imagery. Hence, image fusion of SAR and OPT images can result in information-rich images that can address the challenges in using SAR images for deep learning to perform image classification [5].

A. SYNTHETIC APERTURE RADAR

Synthetic Aperture Radar (SAR) is a type of radar where 2D images are obtained from 3D objects or reconstructions of 3D objects such as terrain surfaces and water bodies are made from their 2D images [6]. SAR imagery is an active data collection method where the sensor produces energy waves to illuminate the target surface and the amount of energy reflected by the target is recorded. Unlike optical image sensors, the SAR sensor gathers the response of the target's surface characteristics such as structure, moisture, and depth.

SAR sensors are capable of producing images with microwave frequencies with the help of a processing method that mimics a long antenna aperture [7]. Hence the antenna is named a 'synthetic aperture.' The microwave range frequency is preferred over other frequencies as the signals can penetrate clouds to reach the target surface. SAR sensor is generally fixed on a rigid platform in motion, such as a spacecraft or a high-altitude aircraft, and the linear and angular movement of the radar antenna is used to scan the target surface. SAR provides a higher spatial resolution than in the case of stationary beam-scanning radars [8]. However, to take advantage of SAR images, a few challenges are to be overcome in comparison to using optical imagery. SAR images are difficult to comprehend as they look different when compared to optical Earth observation images, as shown in Fig. 1. However, the increase in data availability, together with the development of more powerful computing devices, allows the use of SAR imagery for remote sensing and terrain study [9]. Table 1 provides the advantages and limitations in using SAR images.

TABLE 1. Advantages and limitations of SAR images over optical remotely sensed images.

Advantages of SAR imagery	Limitations of SAR imagery
Sensitive to man-made objects	Topographic effects
Independent of external illumination	Difficulty in interpreting image data
Independent of weather condition	Complex processing
Can detect objects with dielectric properties	Speckle effects
Can depict surface depths	Effect of surface roughness

B. DEEP LEARNING AND SAR DATA

SAR data differs to a large extent from optical remote sensing data due to the underlying technology used in the image [5]. The challenges encountered with SAR data for deep learning applications are as follows:

1) Dynamic range and asymmetricity

The dynamic range of a SAR image could be up to 90 dB, depending on the spatial resolution. Also, a typical SAR image has most pixel values in the low amplitude range with bright discrete scatters resulting in a long tail. Such a highly asymmetric scattered distribution of the SAR image data poses a challenge. CNNs cannot handle image data with high dynamic ranges. Hence, most of the existing methods use dynamic compression as a step prior to the processing step. One method to achieve dynamic compression is the amplitude deviation method [10] wherein amplitude values ranging from 0 to 255 are taken and are subtracted by the mean values of each image. Another method to achieve dynamic compression is by using normalization [11], [12].

2) Signal speckle statistics

The speckle nature of the SAR data should be considered while recovering features, namely amplitude and intensity values from SAR images. Since the speckle is the result of a multiplication operation, processing image data with a speckle is a difficult task. Logarithmic operations that reduce multiplication operations to simple addition operations are used as a pre-processing step to overcome the impact of speckle noise in CNNs [13], [14]. However, a single convolutional layer can emulate only approximations to optimum SAR feature estimators. Alternatively, the application of a sophisticated speckle reduction filter, such as non-local averaging, is used as an initial step before using CNN [15]–[17].

3) Imaging geometry

The directional references such as azimuth, coordinates, and SAR image range are not arbitrary. Layovers and shadows that occur at the near range and the far range, respectively, pose a further challenge.

4) Simulation-based training and validation data

Training CNN with remotely sensed data requires validating the data with ground truth. However, obtaining ground truth is the most challenging task due to the lack of data availability. An alternate way is to simulate SAR data to train and validate neural networks. The method is suitable for the reduction of speckles and denoising. However, by adopting such methods, the learning method for the neural networks becomes very simplified for any practical use.

Due to the challenges mentioned above, using SAR images alone for deep learning is challenging. Data preprocessing techniques such as improving the image quality and image fusion techniques to combine SAR and OPT images are used to improve the efficiency of the overall remote sensing applications. This paper proposes quantum processing techniques to process SAR and OPT image pairs and achieve quality improvement in the processed data. Further, we used the processed images to train deep learning models.

The remaining of the paper is organized as follows: Section II describes the motivation behind our work and enumerates the list of contributions. The related work performed in the area of image fusion of SAR and OPT is provided in Section III along with an emphasis on work related to quantum computing. Section IV presents the details of the dataset we created by collecting images from Google Earth Engine. The details of the proposed quantum processing of SAR images, OPT images, and image fusion techniques are provided in Section V. Evaluation of the quality metrics for the processed images is discussed in Section VI. Performance analysis of the deep learning models using the processed images is given in Section VII. Finally, in Section VIII, we conclude our work with future opportunities.

II. MOTIVATION AND CONTRIBUTION

Fusion of SAR images with optical images improves the quality of them for further use [19]. The fused image can overcome the challenges faced by CNNs in handling SAR images alone for remote sensing applications such as scene classification [5]. Although wide variety of classical image fusion techniques are available, there exists a necessity to explore new opportunities provided by recently developed and emerging technologies.

Quantum computing is an emerging field with qubits as information processing units. Qubits are fundamentally different from classical bits as quantum-mechanical properties such as superposition and entanglement are exhibited by qubits [20], [21]. Quantum operations can be performed on qubits to process the information. Finally, measurement is

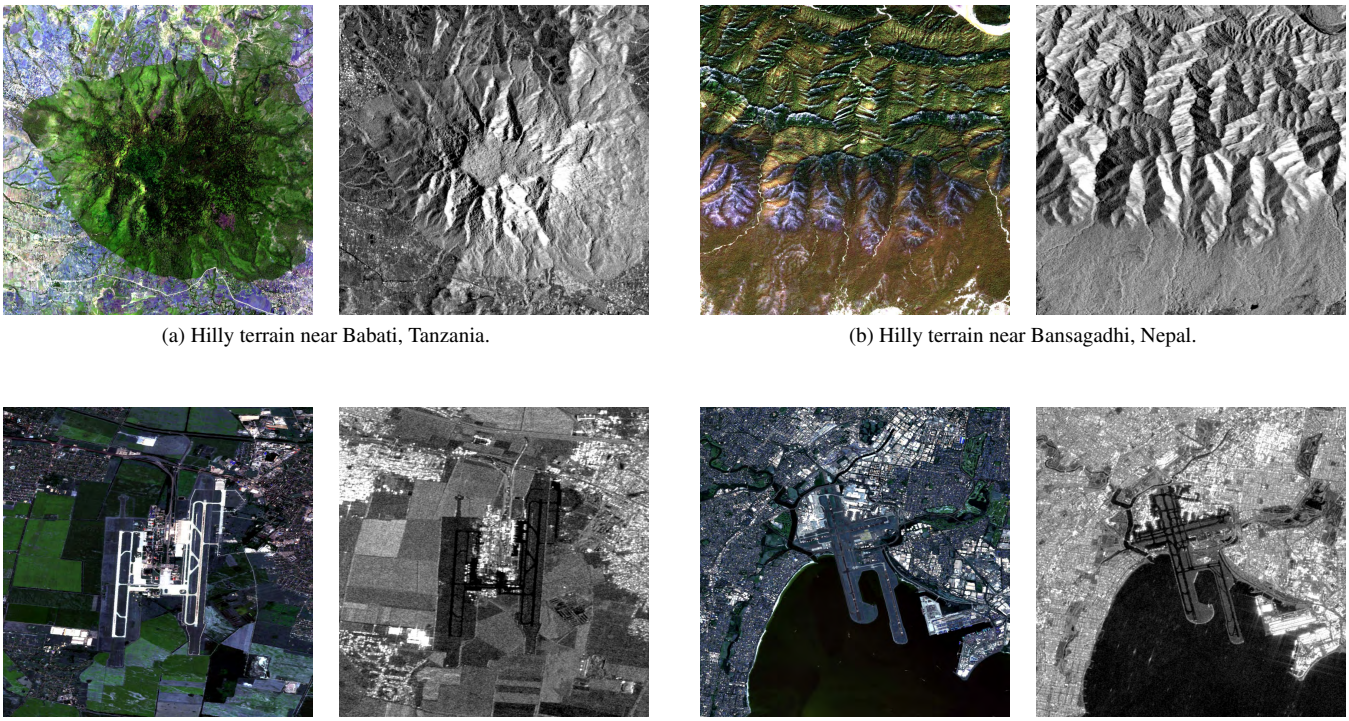

(a) Hilly terrain near Babati, Tanzania.

(b) Hilly terrain near Bansagadhi, Nepal.

(c) Boryspil International Airport, Ukraine.

(d) Sydney (Kingsford Smith) Airport, Australia.

FIGURE 2. Sample optical and SAR image pairs of two classes from the dataset [18] (left - optical & right - SAR in each pair).

performed to obtain a real value. As qubits process information in N-dimensional Hilbert space, different output values can be obtained with quantum processing than that can be obtained in classical processing.

In this paper, we designed a novel approach for the fusion of SAR and optical images. Quantum processing techniques are used to perform image fusion. The fused images are used for the training of computational models using CNNs. Our primary focus is to explore the ability of quantum computing in the area of image fusion for training deep learning models using processed images. The main contributions of our work are as follows:

1) Proposed quantum circuits with quantum operations to process SAR images.
2) Created a dataset suitable for land-use classification remote sensing applications with both SAR images and corresponding optical images collected through Google Earth Engine [22].
3) Proposed two classical processing techniques and eight quantum processing techniques to process and fuse SAR and optical image pairs.
4) Evaluated and analyzed the quality metrics of the output images from the proposed image fusion techniques compared to classical image fusion techniques.
5) Performed a detailed study on the performance of the output images on CNNs for scene classification.

III. RELATED WORK

Image fusion techniques are used to process images and merge the pixel data to obtain a new image and improved image in terms of information [23]. In the process of image fusion, the spectral information of one image can also be combined with the spatial information of another image [24]. Fusion techniques are also used to sharpen the images [25] and enhance specific features that are not visible using a single data [26]. Also, image fusion techniques exist to improve the missing information using different image sensor information and enhancing the images [27].

With the rapid increase in deployment of image data acquisition systems and platforms by various countries and agencies, tremendous amounts of data are being generated and collected. However, using SAR images for deep learning is challenging. Image fusion is used as a preprocessing technique for deep learning. As information can be enhanced in the fused output images, models can learn better with good accuracy [5]. Different mathematical functions can be used to process and combine information from various images to create a new image with improved quality [19]. Hence, image fusion is a crucial data preprocessing technique for several remote sensing applications such as scene classification, terrain analysis, and earth observation [28].

Quantum computers are devices that use quantum mechanical properties to solve complex problems that are difficult to solve using classical computers alone. Quantum supremacy is proved for specific applications where problems that are

TABLE 2. Satellite instrument parameters used for collection of SAR and optical images using GEE.

Remote sensing instrument specifications	Details of parameter options chosen in Google Earth Engine	
Instrument Name	**Sentinel-1 SAR**	**Sentinel-2 MSI**
Acquisition Mode	Interferometric Wide swath (IW)	Wide swath (W)
Format Level	Level-1 (GRD)	Level-2A (Orthorectified)
Spatial Resolution	10 meters	10 meters
Time Period	Jan 1, 2022 - April 1, 2022	Jan 1, 2022 - April 1, 2022
Spectral bands	C-band	Red, Green, and Blue
Polarization	Single polarization (VV)	-
Cloud Coverage in images	-	<1%

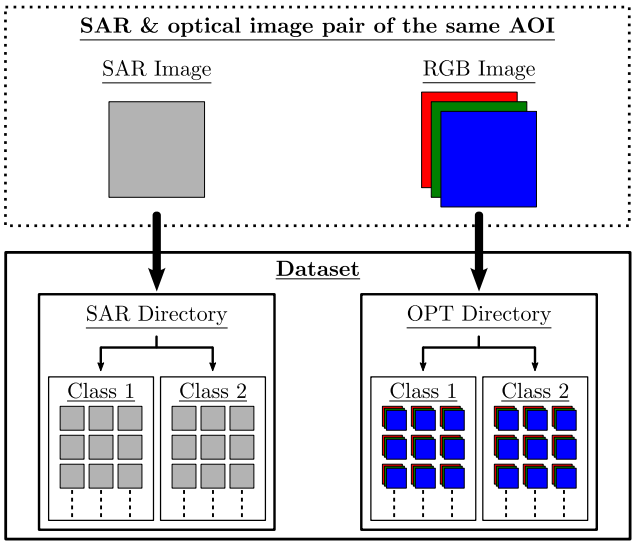

FIGURE 3. Directory organization of the dataset.

difficult for a classical computer to solve are handled very efficiently on a quantum computer [29]. Also, exponential time improvements [30]–[32] over the classical algorithms can be obtained using both supervised and unsupervised quantum machine learning algorithms [33], [34]. In this paper, we utilize the ability of quantum computers to process SAR images for fusion with optical images. The details of the proposed quantum processing techniques for image fusion are presented in the following sections.

IV. DATASET FOR IMAGE FUSION

Here we present the details of the dataset collected for image fusion and deep learning experiments. The dataset is comprised of SAR and OPT satellite images collected from Sentinel-1 and Sentinel-2 satellites. Our dataset is different from the existing datasets. The existing datasets do not provide SAR – Optical image pairs of the same tile area and time with a flexible spatial resolution. Hence, we created an image dataset of two classes with 200 training images (100 SAR – 100 OPT image pairs) for quantum processing, image fusion, and deep learning. Sample image pairs with each class of the dataset are provided in Fig 2.

A. STEPS FOR DATA COLLECTION

In our work, we collected remotely sensed imagery from Copernicus Sentinel through Google Earth Engine (GEE) [22]. The SAR imagery are collected using Sentinel-1 Synthetic Aperture Radar (SAR) instrument [35], [36]. The Optical imagery of the same area and time spans are collected using the Sentinel-2 Multispectral Instrument (MSI) instrument [37], [38]. Further information regarding the remote sensing instruments is provided in Table 2. The entire procedure of collection of image data through GEE and their classification is done in the following seven steps:

Step 1: Specific areas of interest are decided and the approximate geographic coordinates are noted.

Step 2: An accurate area of interest (AOI) is generated based on noted coordinates.

Step 3: A square tile of fixed size (1024 x 1024 pixels) is generated around the area of interest.

Step 4: The standard parameters as shown in Table 2 are chosen for Sentinel-1 and Sentinel-2 instruments.

Step 5: An image with *VV* polarisation from Sentinel-1 and an image with RGB bands from Sentinel-2 are sorted.

Step 6: The two sorted image pairs of the same AOI are exported to cloud storage in GeoTIFF format with a scale of 10.

Step 7: To improve the compatibility with web and non-web based programs, GeoTIFF image pairs are converted to PNG format.

In Step 1, coordinates are selected manually to include the AOI in the dataset suitable for scene classification. For example, we selected different coordinates covering urban areas around airports to create one class of images in the dataset. Steps 2 to 6 are automated using the Python code in GEE. Finally, Step 7 is performed using a web-based IDE such as Google Colaboratory [39]. The converted PNG images are labeled into two classes, as shown in Fig. 3. The detailed organization, description, and availability of the dataset used for our work are provided in [18]. The possible applications of the dataset are land-use classification, scene classification, and deforestation detection. In our work, we performed scene classification where the image scenes are classified based on the category. Scene classification is different from object identification where CNNs use the layout of various objects within the scene for classification [40].

TABLE 3. Quantum circuit used for processing satellite images.

Type of Module	Quantum Circuit (QC)	Mathematical Fusion Function (MF)
Processing Module - I	1− Wired Quantum Circuit 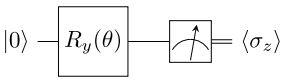 4− Wired Quantum Circuit 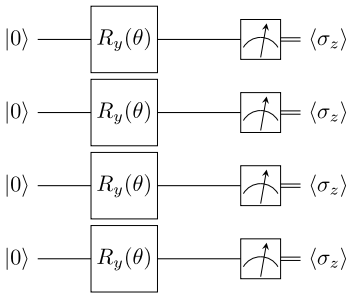	MF $= \frac{3s+r+g+b}{6}$ for QPT_3 to QPT_6 MF $= \frac{3s+m}{4}$ for QPT_7 MF $= \text{stack}(r_f, g_f, b_f)$ for QPT_8 where, $r_f = \frac{s+r}{2}$ $g_f = \frac{s+g}{2}$ $b_f = \frac{s+b}{2}$
Processing Module - II	1− Wired Quantum Circuit 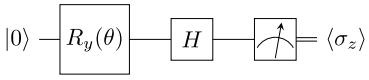 4− Wired Quantum Circuit 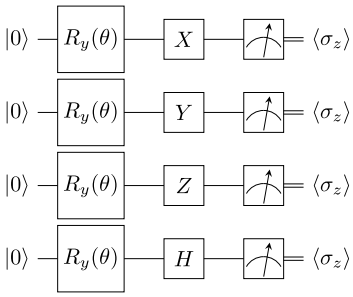	MF = $\frac{s+r+g+b}{4}$ for QPT_3 to QPT_6 MF = $\frac{s+m}{2}$ for QPT_7 MF = $\text{stack}(r_f, g_f, b_f)$ for QPT_8 where, $r_f = \frac{s+3r}{4}$ $g_f = \frac{s+3g}{4}$ $b_f = \frac{s+3b}{4}$

V. QUANTUM PROCESSING FOR IMAGE FUSION

In this section, we present the details of the quantum processing techniques for processing SAR and optical images for fusion. Each image is resized from 1024×1024 to 100×100 due to the limitations in the availability of quantum computational resources. As a preprocessing step, Lee filter [41] is applied on all the SAR images to remove speckle noise.

Encoding classical features into a quantum circuit is a primary step in quantum processing. In our work, the classical data is in the form of images; hence image pixel values in the classical domain are encoded into a quantum circuit. The quantum circuits designed in our work are of two types, one-wired or one qubit-based quantum circuit (1-Wired QC) and four-wired or four qubits-based quantum circuits (4-Wired QC). The two types of circuits differ mainly by the number of output values obtained for a given input value.

In 1-Wired QCs, the ratio of input to output values in the classical domain is 1:1, whereas in 4-Wired QCs, the ratio is 1:4. The quantum circuits designed along with the mathematical functions used in the eight quantum processing techniques (QPTs) are given in Table. 3. Each wire in the quantum circuits represents a qubit. We propose two different processing modules with different mathematical fusion functions for each module.

In *Processing Module - I*, quantum operations in the quantum circuits for all the processing techniques consist of R_y gate operations to accommodate real rotations of the qubits in the Bloch sphere [42]. We used 1-Wired QC and 4-Wired QC in designing quantum circuits, given the limitations of the availability of qubits. Finally, the *Pauli-Z* measurement operator measures the qubit values. The details of the quantum circuits used in our work are given in Table 3. As the output of measurement is a value between $[-1, 1]$, we scale the values to $[0, 255]$ after measurement. The measurement

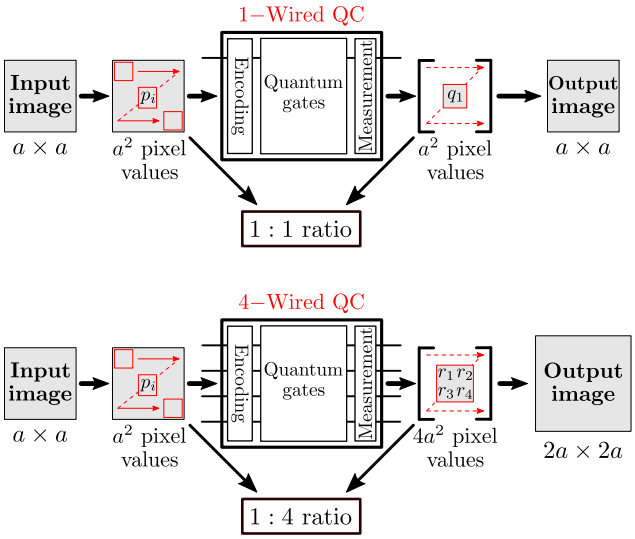

FIGURE 4. Encoding classical image pixel values into a QC.

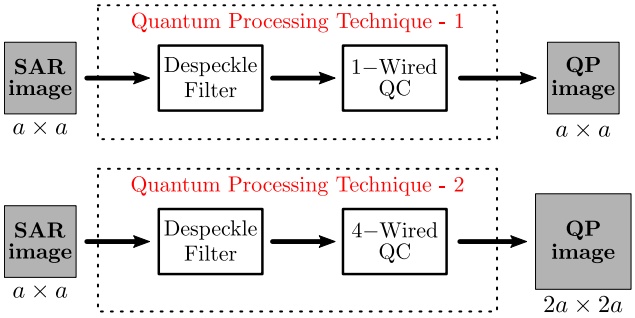

FIGURE 5. QSAR without OPT fusion.

values are used as quantum processed image values.

Quantum operations in *Processing Module - II* consist of further extended operations for the circuits in *Processing Module - I*. We used *Hadamard* gate operation after R_y gate operation for 1-Wired QC. X-gate, Y-gate, Z-gate, and Hadamard gate operations are used after R_y gate operation on the four qubits, respectively, in 4-Wired QC. The operations are extended to obtain different measurement values in comparison with *Processing Module - I*.

In the following, we explain in detail each processing technique and the steps involved. Fig. 4 shows the overall steps involved in the quantum processing of images. All the quantum processing and image fusion techniques are divided into the following categories:

Category-A: Quantum processing of SAR images (QSAR) without image fusion of optical (OPT) images.

Category-B: Quantum processing of SAR images and quantum processing of OPT images (QOPT) followed by image fusion.

Category-C: Image fusion of SAR and OPT images followed by quantum processing.

Category-D: Quantum processing of SAR images and fusion with OPT images.

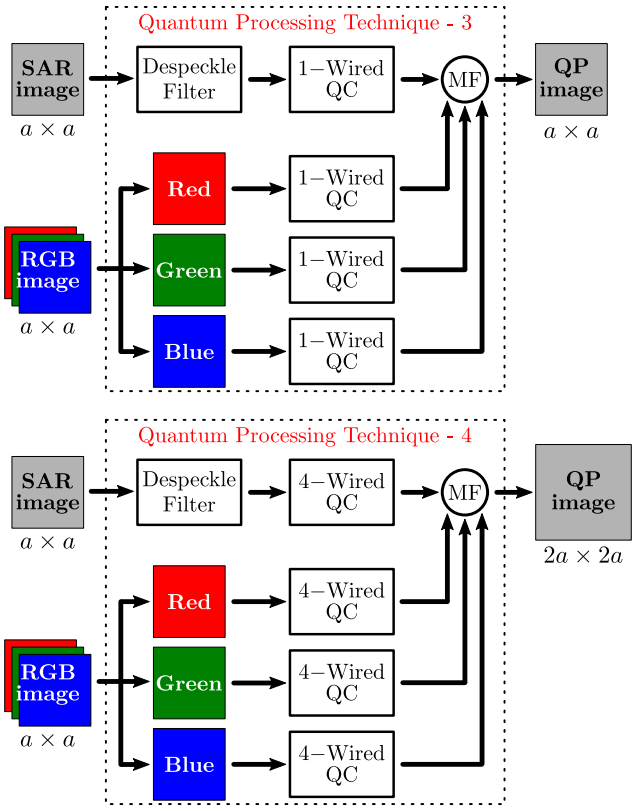

FIGURE 6. QSAR and QOPT followed by fusion.

Processing is performed using both *Processing Module - I* and *Processing Module - II* for all the categories mentioned above. As given in Table 3, mathematical fusion functions in *Processing Module - I* are designed to increased more weightage to the SAR image values. Similarly, OPT image values are given increased weightage in the design of mathematical fusion functions for *Processing Module - II*.

A. QSAR WITHOUT IMAGE FUSION OF OPT IMAGES

In *Category-A*, SAR images are processed using quantum circuits without image fusion with the paired OPT images. In our work, we refer to quantum processing techniques performed in *Category-A* as QPT_1 and QPT_2 as shown in Fig. 5. QPT_1 is based on 1-Wired QC and QPT_2 on 4-Wired QC. Hence, QPT_1 and QPT_2 results in 100×100 and 200×200 sized monochrome images, respectively.

B. QSAR AND QOPT FOLLOWED BY IMAGE FUSION

In *Category-B*, the SAR image and corresponding OPT image are processed using two quantum circuits as shown in Fig. 6. Image fusion is performed after quantum processing with a mathematical function as shown in Table 3. Fig. 6 shows that QPT_3 and QPT_4 differ in the number of wires used in the quantum circuits and hence differ in the final processed monochrome image sizes of 100×100 and 200×200, respectively.

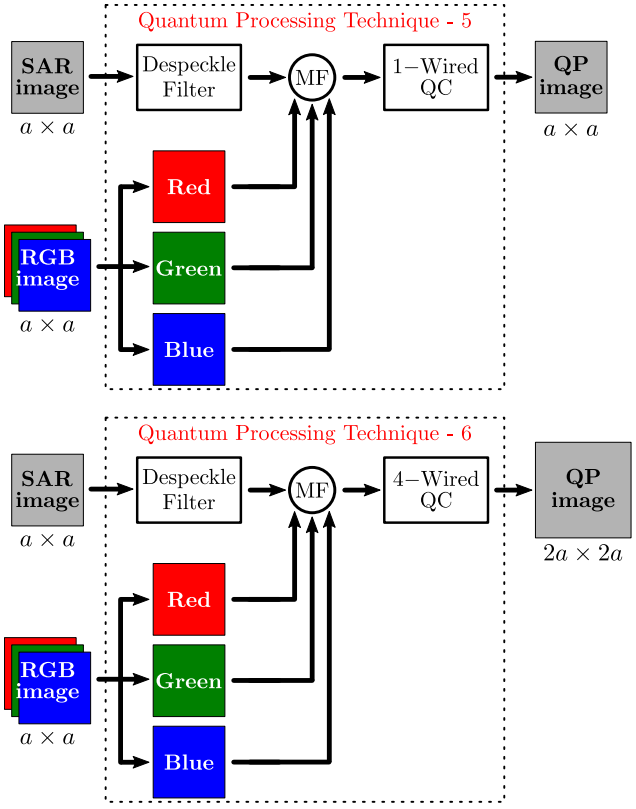

FIGURE 7. SAR and OPT fusion followed by QC.

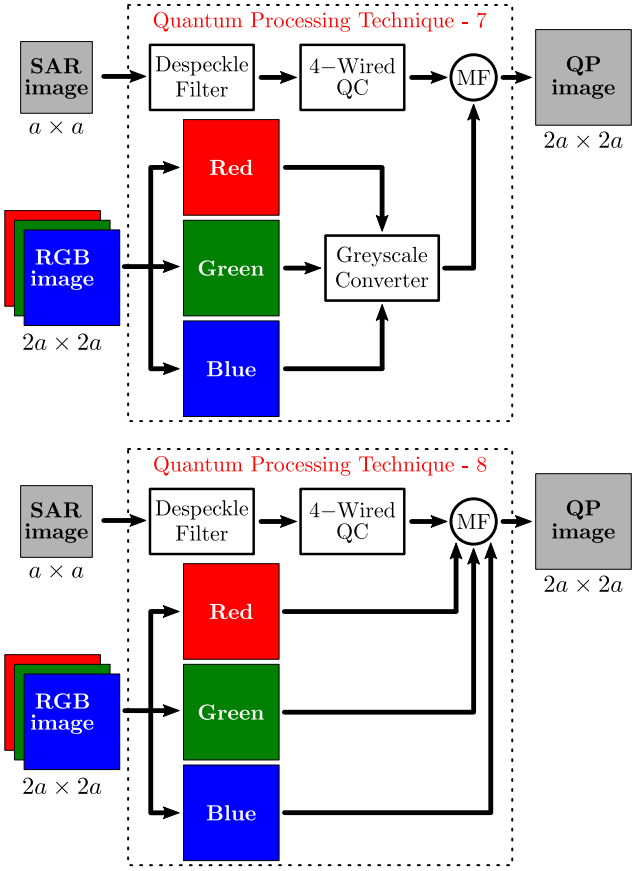

FIGURE 8. QSAR followed by fusion with OPT.

C. SAR AND OPT IMAGE FUSION FOLLOWED BY QUANTUM PROCESSING

In *Category-C*, image fusion is done prior to quantum processing. In the first step, the SAR image and corresponding optical image are fused using the mathematical fusion function given in Table 3. The fused images are then processed using the two different quantum circuits as shown in Fig. 7. The final processed monochrome image sizes for QPT_5 and QPT_6 are 100×100 and 200×200, respectively.

D. QSAR AND FUSION WITH OPT IMAGES

Finally, in *Category-D*, the SAR image alone is processed prior to image fusion with OPT image. In contrast, the OPT image is not processed prior to fusion. *Category-D* consists of two techniques, namely QPT_7 and QPT_8 as shown in Fig. 8. In QPT_7, the OPT image is converted to a grayscale image. In contrast, in QPT_8, the OPT image is used without any grayscale conversion. The optical images in both QPT_7 and QPT_8 are then fused with the quantum processed SAR image using the mathematical fusion function given in Table 3. Even though the size of processed images obtained from QPT_7 and QPT_8 consists of the same size of 200×200, the QPT_8 is a three-layered image with Red, Green, and Blue bands, whereas QPT_7 outputs a single-layered monochrome image.

VI. EVALUATION OF PROCESSED IMAGES

Image fusion techniques are very prominent, therefore, several methods exist to fuse different types of images. However, no single image fusion technique is compatible with all images and performs exceptionally well in all scenarios. Hence, quality assessment is necessary for determining the performance of image fusion techniques. Visual analysis is an easy and direct approach for such performance evaluation. However, some of the processed images are not comprehensible visually. Also, due to the absence of ground truth, the assessment of a processed image by visual interpretation is, therefore, subjective and varies from one interpreter to another [24]. Hence, there is a necessity for quality metrics to assess processed images objectively.

In this section, we present in detail the quality metrics used to evaluate the processed SAR-OPT images and performance evaluation of the quantum processed techniques. We also present the evaluation of the proposed techniques in comparison with CPT_1 and CPT_2, two classical fusion techniques. CPT_1 and CPT_2 are entirely classical processing techniques without any quantum operations. CPT_1 is a pixel-level image fusion method that uses a weighted average for fusion [47], [48] as follows:

$$\text{P}_{fused}(i,j) = \frac{w_1 \text{P}_1(i,j) + w_2 \text{P}_2(i,j)}{w_1 + w_2}. \quad (1)$$

TABLE 4. Visual inspection of processed images of a sample SAR-OPT image pair.

Sample SAR & OPT Image Pair	Processing Technique	Processed Images	
	CPT_1		
	CPT_2		
Sample 1024×1024 SAR image  + Sample 1024×1024 OPT image 		*Processing Module - I*	*Processing Module - II*
	QPT_1		
	QPT_2	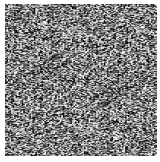	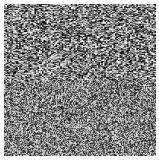
	QPT_3		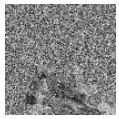
	QPT_4	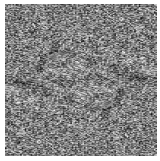	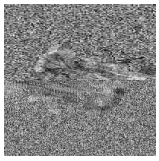
	QPT_5		
	QPT_6	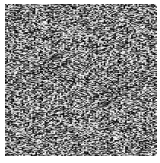	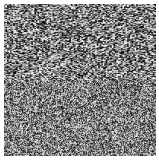
	QPT_7	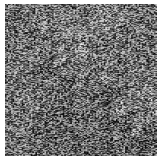	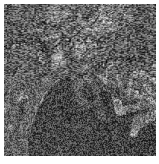
	QPT_8		

TABLE 5. Description of quality metrics used for quantitative evaluation of images.

S. No.	Quality Metrics	Description	Formula	Best value
1	RB	Relative bias (RB) is an absolute value of the difference between mean pixel values of fused and reference images divided by the mean of the reference image [43]. The notations μ_f and μ_r in the formula of RB denote the mean pixel values of fused and reference images, respectively.	$RB = \left(\frac{\lvert\mu_f - \mu_r\rvert}{\mu_r}\right)$	$(value \to 0^+)$
2	RV	Relative variance (RV) is an absolute value of the difference between variance of fused and reference images divided by the variance of reference image [43]. The notations σ_f^2 and σ_f^2 in the formula of RV denote the variance of fused and reference images, respectively.	$RV = \left(\frac{\lvert\sigma_f^2 - \sigma_r^2\rvert}{\sigma_r^2}\right)$	$(value \to 0^+)$
3	$UIQI$	Universal image quality index ($UIQI$) is a measure of image distortion obtained by the multiplication of three components [44]. The first component is loss of correlation between f and r, a measure for similarity between f and r, with a range of $[-1, 1]$. Luminance distortion is the second component with a range of $[0, 1]$. The final factor is contrast distortion and with a range of $[0, 1]$. The notations σ_f^2 and σ_r^2 are variances of f and r; σ_{fr} is covarience of f and r; $\overline{f}$ and $\overline{r}$ denote the mean values of fused and reference images, respectively.	$UIQI = \frac{4(\sigma_{fr})(\overline{f})(\overline{r})}{\left(\sigma_f^2+\sigma_r^2\right)\left((\overline{f})^2+(\overline{r})^2\right)}$	$(value \to 1^-)$
4	$SSIM$	Structural similarity index measure ($SSIM$) is a measure of local patterns of pixel values between fused and reference images and consists range of $[-1, 1]$. The fusion performance can be directly related to structural details in the fused image [45]. The notations μ_f and μ_r denote the mean pixel values of fused and reference images, respectively; σ_f^2 and σ_r^2 are variances of f and r; σ_{fr} is covarience of f and r; C_1 and C_2 are stabilizing variables.	$SSIM = \frac{(2\mu_f\mu_r+\mathrm{C}_1)(2\sigma_{fr}+\mathrm{C}_2)}{\left(\mu_f^2+\mu_r^2+\mathrm{C}_1\right)\left(\sigma_f^2+\sigma_r^2+\mathrm{C}_2\right)}$	$(value \to 1^-)$
5	SD	Standard deviation (SD) measures the level of contrast in fused images. The contrast in an image is an indicative of information richness [43]. The standard deviation measurement gives better values with noiseless images.	$SD = \sqrt{\sum_{k=0}^{l}\left(k-\overline{k}\right)^2 p(k)}$	*Higher value*
6	H	Entropy (H) measures the information contained in a fused image. The notations L in the formula of H denote the dynamic range of the fused image in gray levels; $p(k)$ denotes the chances of occurrence of k^{th} gray level [45].	$H = -\sum_{k=0}^{L} p(k)\log_2 p(k)$	*Higher value*
7	SF	Spatial frequency (SF) is a measure of overall activity level of a fused image [46]. SF is calculated using row and column frequencies of the fused images.	$SF = \sqrt{\mathrm{RF}^2 + \mathrm{CF}^2}$	*Higher value*

$\mathrm{P}_{fused}(i,j)$ corresponds to the fused image pixel value of $m \times n$ sized fused image where, $0 \leq i \leq m$ and $0 \leq j \leq n$. The $\mathrm{P}_1(i,j)$ and $\mathrm{P}_2(i,j)$ are pixel values of corresponding to SAR image and monochrome version of OPT image, respectively. The vales of weights chosen are $w_1 = 3$ and $w_2 = 1$. The processed image size after CPT_1 is 200×200, indicating that the values of m and n are both equal to 200.

The second classical fusion technique, CPT_2, is performed using discrete wavelet transformation (DWT) using Haar algorithm [49]. DWT is categorized as a multi-scale decomposition approach [50]. Image decomposition, fusion, and image reconstruction are the three main steps in this fusion method. The processed image size after applying CPT_2 is also 200×200.

A. VISUAL EVALUATION

The processed images of a sample SAR-OPT pair are given in Table 4 for assessment on a visual basis. Experimental results of ten different processing techniques for a sample SAR and optical image pair are provided. We can observe that the processed images from CPT_1 and CPT_2 are visually more comprehensible than quantum processing techniques (QPTs). From QPT_1 to QPT_8, the quantum processed images exhibit different patterns. The processed images from QPT_1 to QPT_6 are less comprehensible than processed images from QPT_7 to QPT_8. The processed images of QPT_8 are equally comprehensible compared to the classical processing techniques on a visual basis. Also, the quantum processed images under *Processing Module - I* and *Processing Module -*

TABLE 6. Quality metric results of different techniques for raw and processed images.

Type of Module	Value	Technique	Quality Metrics						
			RB	*RV*	*UIQI*	*SSIM*	*SD*	*H*	*SF*
Classical	Min	*SAR*	0.0	0.0	1.0	1.0	44.3292	4.94677	12.8565
		CPT_1	0.00357	**0.27378**	**0.89203**	0.99999	25.1502	**4.57283**	4.40970
		CPT_2	**0.00032**	0.39107	0.76256	0.99999	**26.1790**	4.46218	**5.11574**
	Avg	*SAR*	0.0	0.0	1.0	1.0	56.3591	5.27007	28.03308
		CPT_1	**0.07174**	**0.51104**	**0.96915**	0.99999	**39.0597**	**4.99337**	**7.84694**
		CPT_2	0.15082	0.60332	0.88501	0.99999	35.04176	4.86901	7.31775
	Max	*SAR*	0.0	0.0	1.0	1.0	71.22405	5.42737	63.8886
		CPT_1	**0.16905**	**0.81701**	**0.99629**	0.99999	**60.69613**	**5.24471**	**12.88492**
		CPT_2	0.37687	0.85357	0.98208	0.99999	54.57104	5.17237	11.86978
Processing Module - I	Min	QPT_1	0.00573	0.61321	0.50728	0.99999	**89.2967**	4.20669	17.8012
		QPT_2	0.00573	0.61321	0.50203	0.99999	**89.2967**	4.20669	**30.7923**
		QPT_3	0.00399	**0.00215**	**0.61330**	0.99999	51.6382	**5.30583**	10.6884
		QPT_4	0.00399	**0.00215**	**0.60324**	0.99999	51.63821	**5.30583**	18.86447
		QPT_5	**0.00120**	0.61918	0.51738	0.99999	89.1100	5.10145	17.7078
		QPT_6	0.00573	0.61321	0.50203	0.99999	**89.2967**	4.20669	**30.7923**
		QPT_7	**0.00197**	**0.00529**	**0.56893**	0.99999	68.1828	**5.29044**	**24.4017**
		QPT_8	**0.00307**	**0.00089**	0.55744	0.99999	47.4102	5.13897	16.7657
	Avg	QPT_1	0.13887	1.61612	0.68715	0.99999	**90.3005**	4.81649	17.9982
		QPT_2	0.13887	1.61612	0.67059	0.99999	**90.3005**	4.81649	**31.1052**
		QPT_3	0.14061	**0.16159**	**0.79865**	0.99999	52.2855	**5.32117**	10.7997
		QPT_4	0.14061	**0.16159**	**0.77869**	0.99999	52.2855	**5.32117**	19.1072
		QPT_5	**0.13851**	1.60715	0.69028	0.99999	**90.1474**	5.24180	17.9784
		QPT_6	**0.13887**	1.61612	0.67059	0.99999	**90.3005**	4.81649	**31.1052**
		QPT_7	**0.11303**	0.52185	0.71987	0.99999	68.8451	**5.39933**	**24.6975**
		QPT_8	0.14441	**0.17144**	**0.73654**	0.99999	51.9672	5.29419	17.2289
	Max	QPT_1	0.54515	3.18640	0.79319	0.99999	**91.1256**	5.00854	18.1554
		QPT_2	0.54515	3.18640	0.77569	0.99999	**91.1256**	5.00854	**31.4397**
		QPT_3	0.55199	**0.45781**	**0.90937**	0.99999	53.3553	**5.34443**	11.0556
		QPT_4	0.55199	**0.45781**	**0.89382**	0.99999	53.3553	**5.34443**	19.5867
		QPT_5	**0.53676**	3.17650	0.78792	0.99999	90.8499	5.30192	18.1444
		QPT_6	0.54515	3.18640	0.77569	0.99999	**91.1256**	5.00854	**31.4397**
		QPT_7	**0.49049**	1.42114	0.84376	0.99999	70.7809	**5.48533**	**24.9993**
		QPT_8	**0.46170**	**0.46793**	**0.89302**	0.99999	60.4441	**5.42906**	17.9161
Processing Module - II	Min	QPT_1	0.00315	0.59198	0.51739	0.99999	89.1797	4.18440	17.7561
		QPT_2	0.00205	0.60794	0.50600	0.99999	**89.7366**	4.59131	**33.4949**
		QPT_3	0.00185	**0.01460**	**0.63357**	0.99999	44.3682	**5.19137**	8.68822
		QPT_4	**0.00145**	**0.01019**	**0.61966**	0.99999	44.6283	**5.20711**	16.8916
		QPT_5	**0.00002**	0.61967	0.51380	0.99999	**89.2120**	4.88036	17.0514
		QPT_6	0.00205	0.60794	0.50600	0.99999	**89.7366**	4.59131	**33.4949**
		QPT_7	**0.00005**	**0.00415**	**0.55701**	0.99999	46.7274	**5.09889**	**17.8270**
		QPT_8	0.00616	0.05079	0.42003	0.99999	30.7449	4.83460	10.2142
	Avg	QPT_1	0.13991	1.60027	0.68958	0.99999	90.0249	4.69694	17.9625
		QPT_2	**0.13951**	1.61237	0.67167	0.99999	**90.2357**	5.06104	**33.7018**
		QPT_3	0.14012	**0.34868**	**0.81671**	0.99999	45.0668	**5.20664**	9.31186
		QPT_4	**0.13888**	**0.33895**	**0.79480**	0.99999	45.4156	**5.22239**	17.6273
		QPT_5	0.13974	1.60828	0.68989	0.99999	**90.1648**	5.16402	17.9576
		QPT_6	**0.13951**	1.61237	0.67167	0.99999	**90.2357**	5.06104	**33.7018**
		QPT_7	0.14047	**0.18257**	**0.74077**	0.99999	51.4566	**5.27646**	**18.1957**
		QPT_8	0.21548	0.36925	0.70372	0.99999	44.5853	5.15357	11.3949
	Max	QPT_1	0.55429	3.08753	0.79379	0.99999	**91.0264**	4.89246	18.1821
		QPT_2	0.56414	3.16253	0.77422	0.99999	**90.6438**	5.24659	**33.9091**
		QPT_3	0.56215	**0.60913**	**0.93083**	0.99999	46.0654	5.22881	9.49300
		QPT_4	0.56354	**0.59558**	**0.91188**	0.99999	47.3987	**5.26342**	18.3195
		QPT_5	**0.54979**	3.12007	0.79227	0.99999	**91.2315**	5.24203	18.1904
		QPT_6	**0.56414**	3.16253	0.77422	0.99999	**90.6438**	5.24659	**33.9091**
		QPT_7	**0.46622**	**0.47680**	0.90174	0.99999	60.4898	**5.42746**	**19.0087**
		QPT_8	0.57448	0.72276	**0.92053**	0.99999	64.1350	**5.42576**	13.7818

TABLE 7. Training and validation accuracy results of the deep learning models for raw and processed images.

Type of Module	Technique	Training Accuracy (%)	Validation Accuracy (%)
Classical	*SAR*	86.34	83.23
	CPT_1	**87.87**	**86.25**
	CPT_2	86.22	84.89
Processing Module - I	QPT_1	80.71	72.33
	QPT_2	82.73	75.62
	QPT_3	83.82	81.37
	QPT_4	86.64	82.35
	QPT_5	86.04	82.65
	QPT_6	**89.55**	**86.89**
	QPT_7	**91.10**	**89.70**
	QPT_8	**95.66**	**93.74**
Processing Module - II	QPT_1	90.62	84.63
	QPT_2	91.75	85.12
	QPT_3	95.31	90.68
	QPT_4	96.88	91.75
	QPT_5	96.44	90.70
	QPT_6	**96.44**	**90.70**
	QPT_7	**98.56**	**93.08**
	QPT_8	**98.56**	**97.56**

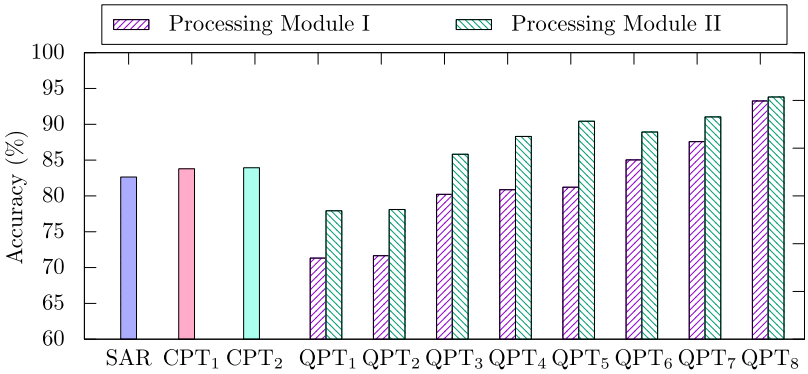

FIGURE 9. Comparison of test accuracies of raw and processed images on deep learning models.

II are visually different due to the difference in the quantum circuits and mathematical fusion functions.

The processed images under *Processing Module - II* are visually more comprehensible than the images from *Processing Module - I*. Images from QPT_7 and QPT_8 of *Processing Module - II* consist of more visual details of land and ocean mass than of *Processing Module - I*. Hence, we can say that quantum operations and mathematical fusion functions are crucial parameters in all quantum processing techniques. The patterns in the processed images are clearly distinguishable from QPT_3 due to the fusion of RGB components, which implies mathematical fusion functions play a crucial role in forming visible patterns in the processed images. QPT_1 and QPT_2 are free of the post-quantum processing fusion method. Hence, there is no mathematical fusion function for the two processing techniques. However, the processed images are visually different in *Processing Module - I* and *Processing Module - II* for QPT_1 and QPT_2 due to the difference in quantum operations.

B. QUANTITATIVE EVALUATION

Visual assessment is subjective and not the best method to assess the processed images. Significantly, the processed images in our work are hard to comprehend. As we use these processed images to train deep learning models, quantitative (objective) evaluation is necessary. In Table 5, we provide the details of the different quality metrics (quantitative evaluation methods) used to evaluate the processed images.

The methods used to assess images are classified into two main categories. In the first category, a reference image is required to evaluate processed images. However, there is no such requirement for a reference image in the second category. As reference image is not always available, methods such as the Wald protocol are used to overcome such a problem [45]. However, a reference SAR image is available in our study. Quantitative evaluation is carried out using some of the well-established quality metrics for SAR-OPT image fusion as explained in detail in Table 5. Quality metrics, namely relative bias (*RB*), relative variance (*RV*), universal

image quality index (*UIQI*), and structural similarity index measurement (*SSIM*) require a reference image for assessment; whereas entropy (*H*), standard deviation (*SD*), and spatial frequency (*SF*) do not require any reference image for the assessment. The seven quality metric values of the images from two classical and eight quantum processing techniques, along with the original SAR image, are provided in Table 6. As 100 output processed images are processed under each processing technique, we provided the minimum, average, and maximum values of each quality metric in Table 6 to analyze the performance of the proposed processing techniques.

Table 6 shows that the *SSIM* values of all classical and quantum processing techniques are very close to 1. Hence, the processed images consists of patterns that are structurally similar to the reference SAR image. *RB*, *RV*, and *UIQI* values show that CPT_1 results greater quality metric values among all other processing techniques. However, the ratio of weights given to SAR and monochrome version of optical image is $3 : 1$ (i.e. $w_1 = 3$ and $w_2 = 1$) of Eqn 1. Therefore, CPT_1 is a direct comparison of 75% SAR image with original SAR image. *RB*, *RV*, and *UIQI* values of quantum processed images are near to the CPT_1 and better than CPT_2. QPT_8 under *Processing Module - I* results the best average value for *RV*.

The *SD* values of both CPT_1 and CPT_2 are less than the *SD* value of original SAR image. Significantly, in the case of quantum processing techniques, *SD* values are higher than the classical processing techniques, irrespective of the processing module. These higher values of *SD* indicate that the level of contrast in processed images using quantum techniques is better than the classical methods. The values of *SD* are highest in QPT_1, QPT_2, QPT_5, and QPT_6, whose values are more than double both classical processing techniques. A similar pattern can be observed in the entropy values of the processed images. CPT_1 and CPT_2 show a decrement in entropy when compared to original SAR images. The quantum processing techniques, on average, show appreciable entropy values. The entropy values are higher in QPT_3, QPT_4, QPT_7, and QPT_8. The higher values of *SD* and entropy in quantum processing techniques, in general, indicate that they are information-rich when compared to the two classical processing techniques and the original SAR image. *SF* values of the processed images using CPT_1 and CPT_2 are less when compared to the values of original SAR images. On the other hand, the quantum processed images show better values than the classical processed images, with QPT_2 and QPT_6 with the highest values.

VII. PERFORMANCE EVALUATION OF DL MODELS

This section presents the details of the performance evaluation of deep learning models on the processed images for scene classification. The experiments are performed using *TensorFlow* package to create CNNs and trained on the processed images along with the original SAR images. Each CNN consists of an input layer, multiple convolution layers, pooling layers, a fully-connected layer, and an output layer equivalent to binary classification. Table 7 shows the training accuracy and validation accuracy comparison of DL models on images processed using the proposed techniques. Fig. 9 shows the test accuracy comparison of the CNNs on different images. The test accuracy of the model trained with original SAR images is 82.64%. The test accuracies with the images obtained from CPT_1 and CPT_2 show minor improvement over with original SAR imagery. However, test accuracies significantly improved using the images from QPT_1 to QPT_8 during training. Specifically, QPT_8 using *Processing Module - I* and *Processing Module - II* outperformed all the other techniques with an accuracy of 93.25% and 95.36%, respectively.

The experimental results also show that the accuracy of the CNNs improved using images that consist of good visually comprehensible features. The accuracy of CNNs trained using images from QPT_1 and QPT_2 solely depends on the quantum circuit operations. The models trained using images from QPT_1 and QPT_2 show limited accuracy compared to other QPTs. Hence, the advantage of SAR and optical image fusion can be observed from the results. QPT_5 and QPT_6 with quantum operations performed after image fusion show better accuracy than QPT_3 and QPT_4, where quantum operations are performed before image fusion. Overall, the accuracy of the models improved using *Processing Module - II* in comparison with the *Processing Module - I*. Hence, the results from Table 6, Table 7, and Fig. 9 show that improving the quality of the data for deep learning models, in turn, improves the overall performance of the models.

VIII. CONCLUSION

Data and model are essential components in any machine learning/deep learning algorithm. Data quality can be crucial in training deep learning models for real-time applications. In remote sensing, many image fusion techniques exist using classical processing to improve data quality. Recently, quantum computing techniques are becoming prominent as information processing on quantum computers is fundamentally different from classical computers. Quantum circuits with quantum operations are used to process information using qubits and obtain output values from measurement.

Our work used quantum computing to process images and proposed image fusion techniques to combine SAR and OPT images. The values from the quantitative evaluation using specific well-established quality metrics indicate that the proposed quantum processing techniques outperform the classical processing techniques. We also evaluated the performance of CNN models using the images obtained from the proposed techniques. Our experimental results show that the accuracy of CNN models improved using the proposed techniques. Hence, quantum processing of SAR images and image fusion with OPT images helps the deep learning models to perform well. Further, different quantum processing techniques can be developed, and the impact of the resultant images on deep learning models can also be studied as the immediate future scope of our work.

REFERENCES

[1] Y. LeCun, Y. Bengio, and G. Hinton, "Deep learning," *nature*, vol. 521, no. 7553, pp. 436–444, 2015.

[2] N. Sambasivan, S. Kapania, H. Highfill, D. Akrong, P. Paritosh, and L. M. Aroyo, "âĂIJeveryone wants to do the model work, not the data workâĂİ: Data cascades in high-stakes ai," in *proceedings of the 2021 CHI Conference on Human Factors in Computing Systems*, 2021, pp. 1–15.

[3] L. J. Miranda, "Towards data-centric machine learning: a short review," *ljvmiranda921.github.io*, 2021. [Online]. Available: https://ljvmiranda921.github.io/notebook/2021/07/30/data-centric-ml/

[4] (2021) A chat with andrew on mlops: From model-centric to data-centric ai - youtube. [Online]. Available: https://www.youtube.com/watch?v=06-AZXmwHjo

[5] X. X. Zhu, S. Montazeri, M. Ali, Y. Hua, Y. Wang, L. Mou, Y. Shi, F. Xu, and R. Bamler, "Deep learning meets sar," *arXiv preprint arXiv:2006.10027*, 2020.

[6] M. Kirscht and C. Rinke, "3d reconstruction of buildings and vegetation from synthetic aperture radar (sar) images." in *MVA*. Citeseer, 1998, pp. 228–231.

[7] L. Cutrona, "Synthetic aperture radar," *Radar handbook*, vol. 2, pp. 2333–2346, 1990.

[8] A. Moreira, P. Prats-Iraola, M. Younis, G. Krieger, I. Hajnsek, and K. P. Papathanassiou, "A tutorial on synthetic aperture radar," *IEEE Geoscience and remote sensing magazine*, vol. 1, no. 1, pp. 6–43, 2013.

[9] M. T. Crockett and D. Long, "An introduction to synthetic aperture radar: A high-resolution alternative to optical imaging," 2013.

[10] M. L. Humber, L. Boschetti, L. Giglio, and C. O. Justice, "Spatial and temporal intercomparison of four global burned area products," *International Journal of Digital Earth*, vol. 12, no. 4, pp. 460–484, 2019.

[11] L. H. Hughes, M. Schmitt, L. Mou, Y. Wang, and X. X. Zhu, "Identifying corresponding patches in sar and optical images with a pseudo-siamese cnn," *IEEE Geoscience and Remote Sensing Letters*, vol. 15, no. 5, pp. 784–788, 2018.

[12] L. Mou, M. Schmitt, Y. Wang, and X. X. Zhu, "A cnn for the identification of corresponding patches in sar and optical imagery of urban scenes," in *2017 Joint Urban Remote Sensing Event (JURSE)*. IEEE, 2017, pp. 1–4.

[13] P. Wang, H. Zhang, and V. M. Patel, "Sar image despeckling using a convolutional neural network," *IEEE Signal Processing Letters*, vol. 24, no. 12, pp. 1763–1767, 2017.

[14] G. Chierchia, D. Cozzolino, G. Poggi, and L. Verdoliva, "Sar image despeckling through convolutional neural networks," in *2017 IEEE International Geoscience and Remote Sensing Symposium (IGARSS)*. IEEE, 2017, pp. 5438–5441.

[15] Y. Shi, X. Zhu, and R. Bamler, "Optimized parallelization of non-local means filter for image noise reduction of insar image," in *2015 IEEE International Conference on Information and Automation*. IEEE, 2015, pp. 1515–1518.

[16] X. X. Zhu, R. Bamler, M. Lachaise, F. Adam, Y. Shi, and M. Eineder, "Improving tandem-x dems by non-local insar filtering," in *EUSAR 2014; 10th European Conference on Synthetic Aperture Radar*. VDE, 2014, pp. 1–4.

[17] L. Denis, C.-A. Deledalle, and F. Tupin, "From patches to deep learning: combining self-similarity and neural networks for sar image despeckling," in *IGARSS 2019-2019 IEEE International Geoscience and Remote Sensing Symposium*. IEEE, 2019, pp. 5113–5116.

[18] M. Sathwik Reddy, C. Avinash, K. Raghavendra, and B. S. Manoj, "Data acquisition and utilization of quantum processed sar and optical images for scene classification," *IEEE TechRxiv Preprint*, May. 2022. [Online]. Available: 10.36227/techrxiv.19672845.v1

[19] S. C. Kulkarni and P. P. Rege, "Pixel level fusion techniques for sar and optical images: A review," *Information Fusion*, vol. 59, pp. 13–29, 2020.

[20] R. P. Feynman *et al.*, "Simulating physics with computers," *Int. j. Theor. phys*, vol. 21, no. 6/7, 1982.

[21] J. D. Hidary, *Quantum Computing: An Applied Approach*. Springer, 2019.

[22] "Google earth engine," https://earthengine.google.com. [Online]. Available: https://earthengine.google.com

[23] M. B. A. Gibril, S. A. Bakar, K. Yao, M. O. Idrees, and B. Pradhan, "Fusion of radarsat-2 and multispectral optical remote sensing data for lulc extraction in a tropical agricultural area," *Geocarto international*, vol. 32, no. 7, pp. 735–748, 2017.

[24] H. Ghassemian, "A review of remote sensing image fusion methods," *Information Fusion*, vol. 32, pp. 75–89, 2016.

[25] X. Meng, H. Shen, H. Li, L. Zhang, and R. Fu, "Review of the pansharpening methods for remote sensing images based on the idea of meta-analysis: Practical discussion and challenges," *Information Fusion*, vol. 46, pp. 102–113, 2019.

[26] A. Sheoran and B. Haack, "Optical and radar data comparison and integration: Kenya example," *Geocarto International*, vol. 29, no. 4, pp. 370–382, 2014.

[27] H. Parikh, S. Patel, and V. Patel, "Classification of sar and polsar images using deep learning: A review," *International Journal of Image and Data Fusion*, vol. 11, no. 1, pp. 1–32, 2020.

[28] H. Kaur, D. Koundal, and V. Kadyan, "Image fusion techniques: a survey," *Archives of Computational Methods in Engineering*, vol. 28, no. 7, pp. 4425–4447, 2021.

[29] F. Arute, K. Arya, R. Babbush, D. Bacon, J. C. Bardin, R. Barends, R. Biswas, S. Boixo, F. G. Brandao, D. A. Buell *et al.*, "Quantum supremacy using a programmable superconducting processor," *Nature*, vol. 574, no. 7779, pp. 505–510, 2019.

[30] L. K. Grover, "Quantum mechanics helps in searching for a needle in a haystack," *Physical review letters*, vol. 79, no. 2, p. 325, 1997.

[31] P. W. Shor, "Polynomial-time algorithms for prime factorization and discrete logarithms on a quantum computer," *SIAM review*, vol. 41, no. 2, pp. 303–332, 1999.

[32] A. W. Harrow, A. Hassidim, and S. Lloyd, "Quantum algorithm for linear systems of equations," *Physical review letters*, vol. 103, no. 15, p. 150502, 2009.

[33] S. Lloyd, M. Mohseni, and P. Rebentrost, "Quantum algorithms for supervised and unsupervised machine learning," 2013.

[34] J. Biamonte, P. Wittek, N. Pancotti, P. Rebentrost, N. Wiebe, and S. Lloyd, "Quantum machine learning," *Nature*, vol. 549, no. 7671, p. 195, 2017.

[35] "User guides – sentinel-1 sar – sentinel online," https://sentinel.esa.int/web/sentinel/user-guides/sentinel-1-sar.

[36] "Sentinel-1 sar - technical guide - sentinel online - sentinel online," https://sentinels.copernicus.eu/web/sentinel/technical-guides/sentinel-1-sar, (Accessed on 04/30/2022).

[37] "User guides – sentinel-2 msi – sentinel online," https://sentinel.esa.int/web/sentinel/user-guides/sentinel-2-msi.

[38] "Sentinel-2 msi - technical guide - sentinel online - sentinel online," https://sentinels.copernicus.eu/web/sentinel/technical-guides/sentinel-2-msi, (Accessed on 04/30/2022).

[39] "Welcome to colaboratory - colaboratory," https://colab.research.google.com/?utm_source=scs-index, (Accessed on 04/30/2022).

[40] J. King, V. Kishore, and F. Ranalli, "Scene classification with convolutional neural networks," *cs231n. stanford. edu*, 2016.

[41] J.-S. Lee, J.-H. Wen, T. L. Ainsworth, K.-S. Chen, and A. J. Chen, "Improved sigma filter for speckle filtering of sar imagery," *IEEE Transactions on Geoscience and Remote Sensing*, vol. 47, no. 1, pp. 202–213, 2008.

[42] O. Gamel, "Entangled bloch spheres: Bloch matrix and two-qubit state space," *Physical Review A*, vol. 93, no. 6, p. 062320, 2016.

[43] L. Wald, T. Ranchin, and M. Mangolini, "Fusion of satellite images of different spatial resolutions: Assessing the quality of resulting images," *Photogrammetric engineering and remote sensing*, vol. 63, no. 6, pp. 691–699, 1997.

[44] Z. Wang and A. C. Bovik, "A universal image quality index," *IEEE signal processing letters*, vol. 9, no. 3, pp. 81–84, 2002.

[45] S. C. Kulkarni and P. P. Rege, "Pixel level fusion techniques for sar and optical images: A review," *Information Fusion*, vol. 59, pp. 13–29, 2020.

[46] A. M. Eskicioglu and P. S. Fisher, "Image quality measures and their performance," *IEEE Transactions on communications*, vol. 43, no. 12, pp. 2959–2965, 1995.

[47] M. Zhu and Y. Yang, "A new image fusion algorithm based on fuzzy logic," in *2008 International Conference on Intelligent Computation Technology and Automation (ICICTA)*, vol. 2. IEEE, 2008, pp. 83–86.

[48] K. Rani and R. Sharma, "Study of different image fusion algorithm," *International journal of Emerging Technology and advanced Engineering*, vol. 3, no. 5, pp. 288–291, 2013.

[49] S. Krishnamoorthy and K. Soman, "Implementation and comparative study of image fusion algorithms," *International Journal of Computer Applications*, vol. 9, no. 2, pp. 25–35, 2010.

[50] Z. Zhang and R. S. Blum, "A categorization of multiscale-decomposition-based image fusion schemes with a performance study for a digital camera application," *Proceedings of the IEEE*, vol. 87, no. 8, pp. 1315–1326, 1999.

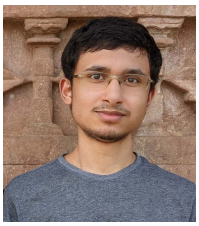

SATHWIK REDDY MAJJI (Student Member, IEEE) is pursuing a bachelor's degree in electronics and communication engineering, Indian Institute of Space Science and Technology (IIST), Thiruvananthapuram, Kerala, India. He is currently a dissertation student in Systems and Networks Lab at IIST. His research interests include quantum machine learning, big data analytics, image processing, and deep learning systems.

AVINASH CHALUMURI (Graduate Student Member, IEEE) received a bachelor's degree in computer science and engineering and a master's degree in computer science and engineering (Data mining) from Jawaharlal Nehru Technological University Kakinada (JNTUK), Andhra Pradesh, India. He is currently a Doctoral Candidate with the Department of Avionics, Indian Institute of Space Science and Technology (IIST), Thiruvananthapuram, India. He serves as a volunteer and an executive member of the IEEE IIST Student Branch. His research interests include quantum machine learning, big data analytics, deep learning, and space quantum internet.

RAGHAVENDRA KUNE received a Ph.D. degree in computer science and engineering from University of Hyderabad (UoH), Telangana, India, in 2016. He is a Scientist 'SG' at Advanced Data Processing Research Institute (ADRIN), Department of Space, Government of India. He is also the head of high-performance computing systems and drones at ADRIN. He is also a member of Astronomical Society of India, Associate member of Andhra Pradesh Academy of Sciences, and a member of Indian National Cartography Association. His research interests include big data analytics, quantum machine learning, deep learning, and remote sensing applications.

B. S. MANOJ (Senior Member, IEEE) received a Ph.D. degree in computer science and engineering from the Indian Institute of Technology Madras in 2004. He was an Assistant Research Scientist and a Lecturer with the Electrical and Computer Engineering Department, University of California at San Diego. He is currently a Professor with the Department of Avionics, Indian Institute of Space Science and Technology, Thiruvananthapuram, India. He also serves as Chair, IEEE EMB Society Kerala Chapter. His current research interests include quantum machine learning, quantum computing, quantum internet, satellite networks, and 6G-satellite integration.